

Rare earths (Ce, Eu) molar concentration-dependent of the structural and optical properties of CBD-CDs nanofilms

J.I. Contreras-Rascón^a, M.E. Linares-Avilés^b, J. Díaz-Reyes^{c,*}, J.F. Sánchez-Ramírez^c, J.E. Flores-Mena^d, R.S. Castillo-Ojeda^e, M.C. Peralta-Clara^c, and J.S. Veloz-Rendón^c

^a*División de Ingenierías, Universidad del Valle de Puebla, 3 Sur 5759. Col. El Cerrito, Puebla, Puebla. 72440. México.*

^b*Unidad Profesional Interdisciplinaria de Biotecnología, Instituto Politécnico Nacional, Av. Acueducto Poniente, La Laguna Ticoman. Ciudad de México. 07340. México.*

^c*Centro de Investigación en Biotecnología Aplicada, Instituto Politécnico Nacional, Ex-Hacienda de San Juan Molino, Km. 1.5. Tepetitla, Tlaxcala. 90700. México.*

*e-mail: joel.diaz_reyes@hotmail.com

^d*Facultad de Ciencias de la Electrónica de la BUAP,*

Av. San Claudio y 18 Sur. Colonia Jardines de San Manuel, Ciudad Universitaria, 72500, Puebla, Puebla, México.

^e*Universidad Politécnica de Pachuca,*

Km. 20, Rancho Luna, Ex-Hacienda de Santa Bárbara, Municipio de Zempoala, Hidalgo. 43830. México.

Received 3 January 2018; accepted 22 February 2018

It presents the characterization of rare earths (Eu,Ce)-doped CdS nanofilms that were synthesised by the growth technique chemical bath deposition (CBD) at the reservoir temperature of $70 \pm 2^\circ\text{C}$. The doping of CdS with rare earths is performed by varying the synthesis time from 60 to 135 min. The rare earths molar concentration was range from $0.0 \leq x \leq 3.5$, which was determined by energy dispersive X-ray spectroscopy. X-ray diffraction (XRD) analysis and Raman scattering reveal that CdS nanofilms showed the zinc blende (ZB) crystalline phase. The CdS average nanocrystal size was ranged from 1.84 to 2.67 nm that was determined by the Debye-Scherrer equation from ZB (111) direction, which was confirmed by transmission electron microscopy. Raman scattering shows that the lattice dynamics is characteristic of bimodal behaviour and the multiplexes adjust of the first optical longitudinal mode for the (Eu,Ce)-doped CdS, which denotes the Raman shift of the characteristic peak about 305 cm^{-1} of the CdS nanocrystals. The CdS nanofilms exhibit a direct bandgap that slightly decreases with increasing doping, from 2.50 to 2.42 eV, which was obtained by room temperature transmittance. The room-temperature photoluminescence of CdS shows the band-to-band transition at 2.88 eV, which is associated to quantum confinement and a dominant radiative band at 2.37 eV that is called the optical signature of interstitial oxygen. The Eu^{3+} -doped CdS photoluminescence shows the dominant radiative band at 2.15 eV, which is associated to the intra-4f radiative transition of Eu^{3+} ions that corresponds to the magnetic dipole transition, ($^5\text{D}_0 \rightarrow ^7\text{F}_1$). For the Ce^{3+} -doped CdS the dominant radiative transition, at 2.06 eV, is clearly redshifted, although the passivation of the CdS nanofilms by Ce was approximately by a factor about 21 for the best results.

Keywords: CdS; Chemical bath deposition; Rare earths; cerium; europium.

Se presenta la caracterización de las nanopelículas de CdS impurificadas con tierras raras (Eu,Ce) que se sintetizaron mediante la técnica de crecimiento deposición de baño químico (CBD) a la temperatura del reservorio de $70 \pm 2^\circ\text{C}$. La impurificación de CdS con tierras raras se realizó variando el tiempo de síntesis de 60 a 135 min. La concentración molar de las tierras raras fue de $0.0 \leq x \leq 3.5$, que se determinó mediante espectroscopia de rayos X de energía dispersiva. El análisis de difracción de rayos X (XRD) y dispersión de Raman revelan que las nanopelículas de CdS mostraron la fase cristalina de zinc blenda (ZB). El tamaño medio de los nanocristales de CdS varió de 1.84 a 2.67 nm, que se determinó mediante la ecuación de Debye-Scherrer a partir de la dirección ZB (111), que se confirmó mediante microscopía electrónica de transmisión. La dispersión Raman muestra que la dinámica de la red es característica del comportamiento bimodal y el ajuste multipicos del primer modo longitudinal óptico para el CdS impurificado con (Eu, Ce), el cual denota el desplazamiento Raman del pico característico en aproximadamente 305 cm^{-1} de los nanocristales de CdS. Las nanopelículas de CdS exhiben una banda prohibida directa que disminuye ligeramente al aumentar la impurificación, de 2.50 a 2.42 eV, que se obtuvo por transmitancia a temperatura ambiente. La fotoluminiscencia a temperatura ambiente de CdS muestra la transición de banda a banda a 2.88 eV, que está asociada al confinamiento cuántico y una banda radiativa dominante a 2.37 eV que se denomina firma óptica del oxígeno intersticial. La fotoluminiscencia de CdS impurificada con Eu^{3+} muestra la banda radiativa dominante a 2.15 eV, que está asociada a la transición de radiación intra-4f de los iones Eu^{3+} que corresponde a la transición del dipolo magnético, ($^5\text{D}_0 \rightarrow ^7\text{F}_1$). Para el CdS impurificado con Ce^{3+} , la transición radiativa dominante, a 2.06 eV, está claramente desplazada hacia el rojo, aunque la pasivación de las nanopelículas de CdS por Ce fue aproximadamente por un factor de 21 para obtener los mejores resultados.

Descriptores: CdS; deposición por baño químico; tierras raras; cerio; europio.

PACS: 81.07.Bc; 81.16.Be; 61.05.cp; 61.46.Df; 61.72.uj; 78.30.Fs; 78.40.Fy; 78.55.Et

1. Introduction

Semiconductor nanostructures have attracted a lot of attention due to their unique mechanical, optical and electronic properties. Inorganic compounds doped with lanthanide ions are widely used as the luminescent materials in lighting [1] and displays [2], optical amplifiers [3] and lasers [4]. Lately, the optical properties of crystal nanomaterials doped with lanthanide impurities have attracted much attention as they are expected to modify both electronic states and optical properties. Consequently, a possible influence of quantum size effect on the luminescence properties is expected for II-VI semiconductor compound nanocrystals due to the inclusion of rare earth (RE) metal ions [5]. The effects of the quantum confinement size of the semiconductor nanoparticles not only create photogenerated carriers, which may have an interaction with f-electrons but also significantly influence the optical properties [6]. Therefore, excitonic transition in the host material and an improvement in the luminescence intensity is also expected for the semiconductor nanostructures after the rare earths (RE) doping. The effects of the reduced dimensionality on the electronic relaxation and the phonon density-of-states of semiconductor compounds and insulating nanocrystals have been extensively investigated by both theoretical and experimental approaches [7,8].

Doping of II-VI semiconductors compounds with rare earths ions like cerium, terbium and europium, etc., has recently been extensively studied [9]. Doping by rare earth elements such as cerium reduces the particle size of the nanomaterials and increases the effective surface area [10]. Vij *et al.* reported the optical property studies on Ce doped SrS nanostructures and Ce doped CaS nanoparticles synthesized by solid state diffusion method [11]. Kumar *et al.* [12] have reported luminescence investigations on Ce³⁺-doped CaS synthesized using the chemical co-precipitation method.

In this work reports the structural and optical characterization of CdS and CdS:(Ce³⁺, Eu³⁺) nanofilms obtained by chemical bath deposition on glass substrate synthesised at 70 ± 2°C at different synthesis times for varying the rare earth molar concentration. The effects of the chemical composition on structural and optical properties of the CdS and CdS:(Ce³⁺, Eu³⁺) were studied by EDS, X-ray diffraction, HRTEM, Raman spectroscopy, transmittance and photoluminescence at room temperature.

2. Experimental details

The growth technique to obtain the CdS doped with rare earth is the chemical bath deposition [13] in its modality of immersion, in which a cryo-thermostat of circulation Polyscience with temperature controller of -40 to 200°C was used. Being graded it at the temperature of 20°C to avoid the release of harmful gases into the environment and using ammonium nitrate as complexing agent. The solutions mixture is carried out using the following precursors: cadmium chloride dehydrate (CdCl₂+2H₂O) (Productos Químicos Monter-

rey S.A.), potassium hydroxide (KOH) (JT Baker, 98.6% purity), Ammonia Nitrate (NH₄(NO₃)) (Sigma-Aldrich, 99.5% purity) and thiourea thiocarbamide (Fermat, 99.9% purity). The nitrifying reagents are europium (III) nitrate pentahydrate (Eu(NO₃)₃+5H₂O) (Sigma-Aldrich, 99.999% purity) and cerium (III) nitrate (Ce(NO₃)₃+6H₂O) (Sigma-Aldrich, 99.999% purity) working with the following concentrations 0.05 M CdCl₂, 0.05 M KOH, 0.1 M NH₄(NO₃), 0.05 M NH₂SCNH₂. The precursor concentrations are Eu(NO₃)₃ 0.001 M and Ce(NO₃)₃ 0.001 M with the appropriate volumes, the doping is achieved when the solutions mixture has a slightly basic pH. The increase in the doping molar concentration is performed by increasing the synthesis time, which was ranged from 60 to 135 min., achieving yellowish-opaque surfaces. The synthesised samples are shown in Table I and the number that accompanies the sample name corresponds to the synthesis time. The CdS:(0, Eu³⁺, Ce³⁺) nanofilms chemical stoichiometry was obtained by Energy Dispersive Spectrometry (EDS), which was carried out in a System LEO 438VP, with W.D. of 26 mm using a pressure of 20 Pa. The crystalline phase and structure of the nanocrystals were determined with a Bruker D8 Discover diffractometer using the copper K α radiation ($\lambda = 1.5406 \text{ \AA}$) at 40 kV and 40 mA with parallel beam geometry. High-resolution transmission electron microscopy (HRTEM) studies were carried out in a JEOL JEM200 of 80-200 kV, the obtained image is recorded with a CCD camera in real time. The Gatan Digital Micrograph software was used for the analysis of HRTEM images. Raman scattering was performed using the 632.8 nm line of a He-Ne laser at normal incidence for excitation. The light was focused to a diameter of 6.0 μm at the sample using a 50 \times (numerical aperture 0.9) microscope objective. The nominal laser power used in these measurements was 20 mW. Scattered light was analysed using a micro-Raman system (Lambram model of Dilor), a holographic notch filter made by Kaiser Optical System, Inc. (model superNotch-Plus), a 256 \times 1024-pixel CCD used as detector cooled to 140 K using liquid nitrogen, and two interchangeable gratings (600 and 1800 g/mm). The room temperature transmittance was performed using a Bruker Infrared Spectrometer Vertex 70. The 300 K photoluminescence was measured using a He-Cd (Omnichrome-Series 56) laser emitting at 325 nm with an optical excitation power of 15 mW. The radiative emission from the sample was focalized to the entrance slit of a HRD-100 Jobin-Yvon double monochromator with a resolution better than 0.05 nm and detected with an Ag-Cs-O Hamamatsu photomultiplier with a spectral response in the range 350-1000 nm.

3. Experimental results and discussion

The chemical stoichiometry of the CdS:RE³⁺ nanofilms was estimated by EDS measurements. Figure 1 shows EDS spectra of two typical samples, M100 and M115. The information of the most elementary elemental composition (spot analysis) was generated by keeping the electron beam fixed at several

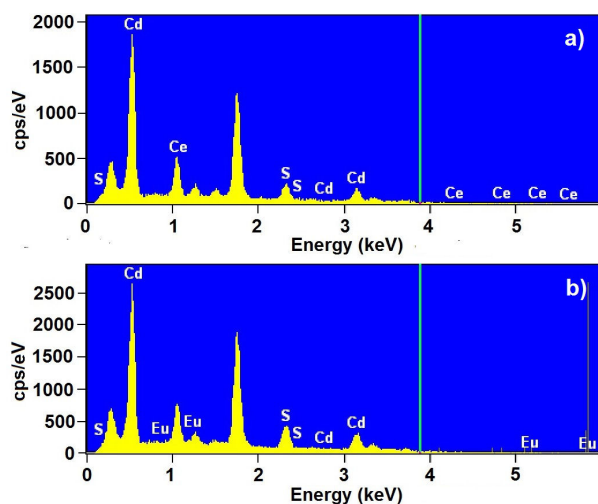


FIGURE 1. EDS spectra of two CdS typical samples, which show clearly the presence of rare earths in the nanofilms: a) M100 and b) M115.

points of the sample, in which the total scan was performed (global analysis), which besides allowed to know the presence of the residual impurities as oxygen in the samples along with cadmium and sulphur. It has been found that oxygen ions are present in the layers in the form of O^{2-} ions, which could produce CdO [14,15]. These oxygen ions form trap levels in the band gap, resulting in several radiative or non-radiative transitions contributing or affecting to the luminescence, since that O^{2-} ions replace sulphur atoms at some random points of the S sub-lattice. The EDS measurements are presented in Table I, in which are included the atomic and mass percentages of the elements. From these results is observed that CdS samples are not stoichiometric. As is known the atomic weight of the ideal unit cell is ~ 288.95 u that corresponds to 22.19% sulphur atoms and 77.81% cadmium atoms. Therefore, if there is excess cadmium and lack of sulphur that is indicative that cadmium is interstitial and there are vacancies of sulphur [16]. Table I shows that the nanofilms contain a lower concentration of sulphur, indicating that have a high concentration of sulphur vacancies. Also, it can induce that there is a high concentration of cadmium and RE interstices [16].

Figure 2 shows X-ray patterns of typical CdS:(Ce,Eu) nanofilms with different rare earths molar concentrations deposited at temperature of $70 \pm 2^\circ\text{C}$, which were synthesised at different times. It is observed from XRD patterns that CdS:RE $^{3+}$ deposited nanofilms are in polycrystalline nature. As can be seen, the diffraction pattern of the M65 sample shows clearly a predominant peak at $2\theta = 26.76^\circ$, which can be assigned to (111) plane of ZB CdS crystalline phase, indicating a preferential growth orientation. In addition, it can be seen that each peak corresponds fairly well with data of CdS marked in the software DICVOL04 data. The lattice constant obtained with the software DICVOL04 data is in good agreement with the published results [16], obtained values of the lattice parameter that are shown in Table II and Fig. 3 that

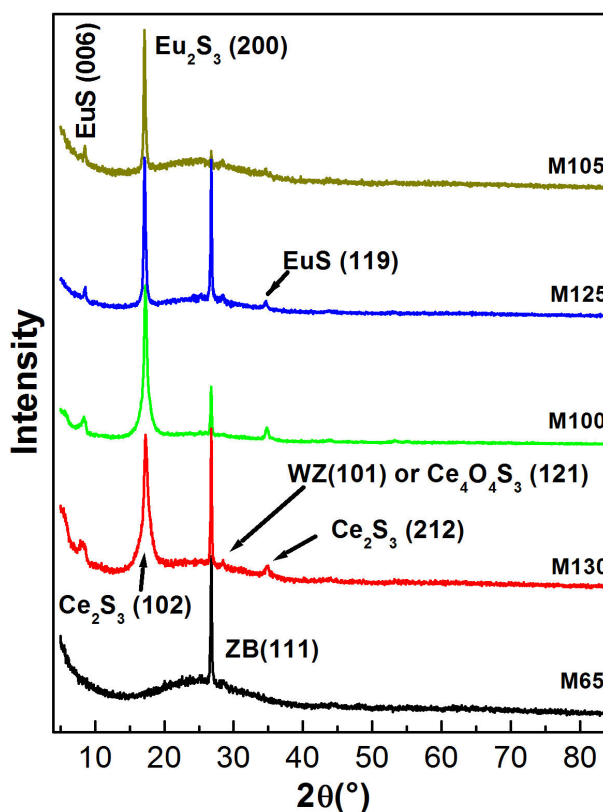


FIGURE 2. XRD diffraction patterns for CdS and CdS:RE $^{3+}$ nanofilms. a) It shows the M65 diffractogram that displays a peak at: $2\theta = 26.78^\circ$. This is related to the (111) diffraction plane for the ZB phase of the CdS. b) and c) They illustrate the CdS:RE $^{3+}$ diffractograms, in which clearly are shown peaks associated at RE at 8.33 and 17.14° . All the diffraction peaks can be perfectly matched to the reference patterns (JDDC 0531447) displaying the ZB crystalline phase.

confirmed that the CdS:RE $^{3+}$ nanofilms for all the molar concentrations belong to face-centered cubic system and their X-ray patterns are described in the $Fm - 3m(225)$. For rare earth doped films diffractograms, the appearing of new diffraction peaks are associated to the incorporation of RE $^{3+}$ at the sub-lattices sites of Cd $^{2+}$. As is clearly seen in Fig. 3 the CdS:Ce $^{3+}$ diffractograms present two dominant diffraction peaks at 17.26 and 26.76° , first one is associated to (102) diffraction plane of Ce $_2$ S $_3$ and the second is assigned to (111) plane of ZB CdS crystalline phase. Besides, two small diffraction peaks at 28.44 and 34.73° that are associated with Ce $_4$ O $_4$ S $_3$ (121) plane and Ce $_2$ S $_3$ (212) plane. Another diffraction peak is observed at 8.45° , which may be associated with CeS. Similarly, X-ray diffraction diffractograms of the CdS:Eu $^{3+}$ films, in addition to (111) plane of ZB CdS crystalline phase at 26.67° present peaks at 8.46 , 17.07 and 34.63° that are associated to the incorporation of the europium. The first one is assigned to the diffraction plane (006) EuS, the second that is the dominant peak is associated with Eu $_2$ S $_3$ (200) diffraction plane and the weak peak is assigned to the EuS (119) diffraction plane. It has been reported that the probability that CdS dissolves in the RE $_2$ S $_3$

TABLE I. It presents the CdS:RE³⁺ synthesised nanofilms and the doping volume added to each one. Additionally, the Cd, S and RE molar concentrations of the nanofilms that were estimated by EDS. The average errors with that were estimated percentage masses of different elements were for cadmium 1.25%, sulphur 0.35%, europium 0.25% and for cerium 0.30%.

Sample	RE(NO ₃) ₃ Added volume (ml)	Cd mass weight (%)	Cd molar fraction (%)	S mass fraction (%)	S molar fraction (%)	RE mass fraction (%)	RE molar fraction (%)
M60	—	80.66	54.32	19.34	45.68	—	—
M65	—	79.20	52.06	20.80	47.94	—	—
M70	—	78.31	50.74	21.69	49.28	—	—
M74	—	77.11	49.01	22.89	50.99	—	—
	Eu(NO ₃) ₃					Eu	Eu
M105	1	80.62	56.79	17.16	42.36	2.23	0.85
M115	2	80.25	57.12	16.71	41.70	3.04	1.18
M125	3	78.98	56.87	16.37	41.32	4.65	1.81
M135	4	71.06	43.10	22.54	47.57	5.86	3.47
	Ce(NO ₃) ₃					Ce	Ce
M80	1	74.55	46.45	24.24	52.95	1.21	0.60
M100	2	75.64	48.01	23.06	51.32	1.31	0.66
M130	3	71.06	44.03	25.26	54.32	3.68	1.65

TABLE II. It presents the lattice constant, interplanar distance and average grain size of the nanofilms obtained by the Debye-Scherrer equation for the ZB (111) preferred direction showing their dependence on the synthesis time of the nanofilms estimated by XRD. Besides. In addition, it presents the grain size obtained by TEM and the interplanar distance estimated by HRTEM.

Sample	a by XRD (Å)	$d_{(111)}$ by XRD (nm)	Grain size by XRD (nm)	Grain size by TEM (nm)	$d_{(111)}$ by HRTEM (nm)
M60	5.76	0.332	2.67	—	—
M65	5.77	0.333	2.46	5.10	0.29
M70	5.83	0.337	2.37	5.44	0.33
M74	5.88	0.339	2.45	—	—
M105	5.84	0.337	1.84	—	—
M115	5.87	0.339	1.88	3.55	0.33
M125	5.86	0.338	1.85	3.50	0.33
M135	5.87	0.339	1.87	—	—
M80	5.88	0.339	1.85	—	—
M100	5.87	0.339	1.84	3.33	0.33
M130	5.81	0.335	2.01	—	—

lattice at room temperature is very low [17] but when increases the molar concentration also is increased the probability, as is observed in the CdS:Re³⁺ X-ray diffractograms. In this case of extremely small particles, as the present case, where the contribution of surface free energy is very important, some deviations cannot be excluded. From XRD patterns can be assured that the RE³⁺ forms RE₂S₃ according to the diffraction peaks. From the XRD study can infer that the formation of the CdS:RE³⁺ occurs in the early stage, following by the formation of RE₂S₃ nanocrystallites in the stage of the film growth [18]. Additionally, it is observed a widening at the diffraction peak of the preferential ZB (111) direc-

tion, which may be caused by size of small crystalline domain and/or fluctuations in chemical composition. The undergoing stress cannot happen since the substrates are amorphous and they do not produce a mismatch in the lattice parameters of layers. Therefore, widening at the diffraction peak occur due to the small size of the crystals and by presence of strains that possess multiple facet diffraction peaks, which is the result of polycrystalline growth of the synthesized nanocrystals. These X-ray diffraction peaks do no match exactly with the reported plane spacing for ZB phase, this difference can be explained by the broadening of peaks due to the small size of the crystals and by presence of strains that possess multiple

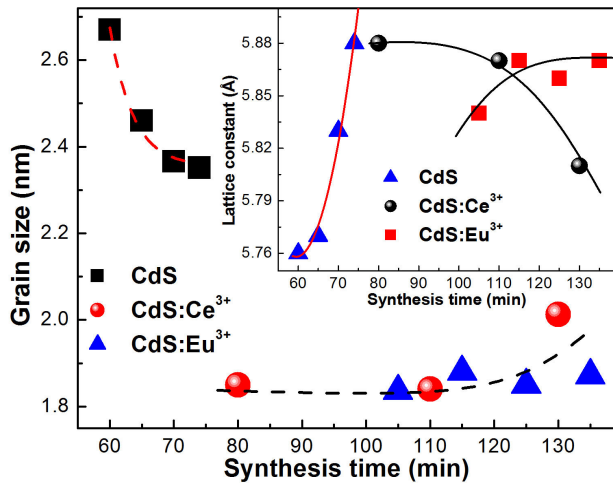


FIGURE 3. It illustrates the average grain size as function of synthesis time for RE-doped CdS nanofilms. The inset shows the lattice parameters for doped CdS nanofilms. The solid lines are some figures-of-merit for following the behaviour of experimental points.

facet diffraction peaks. The nanocrystal size was calculated from the broadening of the peak of the preferential ZB (111) direction of each nanolayer, using the Debye-Scherrer equation [19]. When applying the Debye-Scherrer equation finds that, the crystalline domain presents clearly two behaviour: a) as the synthesis time increases for single CdS nanofilms the average grain size diminishes slightly from 2.97 to 2.35 nm and b) for RE³⁺-doped CdS nanofilms there are a noticeable decrease in the crystalline domain. Although, for Eu³⁺-doped samples there are a slight increase grain size from 1.85 to 2.03 nm and for Eu-doped films do not vary appreciably, remain almost constant from 1.84 to 1.87 nm, by increasing the synthesis time. The results are shown in Fig. 3, where clearly is observed the RE³⁺ ions effect to replace Cd ions of the Cd sub-lattice. A similar behaviour is observed for the lattice constant, as can see in the inset of Fig. 3. For single CdS lattice constant increases slightly as synthesis time is increased, from 5.76 to 5.88 nm, and for the samples doped with cerium (europium) increases (decreases) slightly. For the interplanar distance (ID) (111) of the nanolayer ZB crystalline phase is presented in Table II that was calculated from the 2θ peak position versus synthesis time, which increases slightly. This ID, in practice, coincides with (111) ID of the CdS bulk ZB crystalline phase. It is worth-noting the values of electronegativity for Ce(1.12), Eu(1.2) and Cd(1.69), which are favourable to form a solid solution [20]. It can be seen in Fig. 3 the undoped CdS grain size slightly decreases as synthesis time is increased, suggesting the formation of a solid solution as has been reported [20], presenting a region of discontinuity when is added [RE³⁺] and slightly increases for Ce-doped CdS to a higher dopant concentration. On the other hand, the lattice constant in-

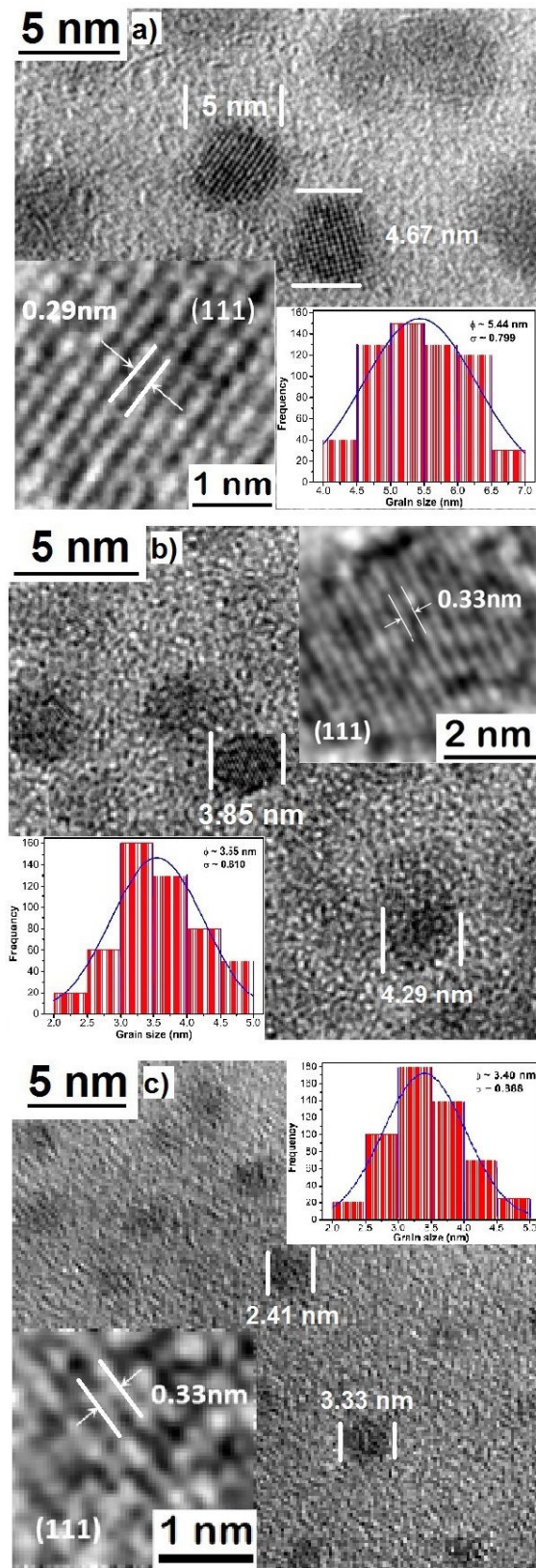


FIGURE 4. TEM micrographs of the typical CdS samples: a) M60, b) M115 and c) M100. Additionally, in the insets HRTEM micrographs and histograms are shown, which allow to estimate the interplanar distance and grain size of the nanoparticles.

creases lightly with increasing synthesis time and happens a discontinuity when is added $V[RE^{3+}]$ in the nanofilms, which is an effect of RE^{3+} substituting Cd^{2+} in CdS lattice. A possible explication to this observed experimental fact can be due to difference of the ionic radii of Cd^{2+} (0.97 Å) and Ce^{3+} (1.15 Å) and Eu^{3+} (1.09 Å). The (111) ID of ZB cubic phase of CdS bulk is 0.3367 nm, this value is light lower than the ID values found for the CdS-CdS:RE nanofilms in this work [20]. It is probable that ID values in CdS:RE³⁺ nanofilms are owing to the existence of Cd^{2+} vacancies. For a relative low concentration of RE^{3+} ions, this can be, in a large majority of the samples, be situated in: (a) Cd^{2+} vacancies sites that otherwise would be empty [21], (b) in Cd^{2+} sites provoking the appearing of Cd^{2+} interstitial, and (c) in interstitial positions. For higher synthesis times, that is higher $V[RE^{3+}]$, the material behaves like a solid solution, the generation of Cd^{2+} vacancies, whose creation is needed to charge balance, starts to be important in number and given the relative ionic radius of S^{2-} . There is a tendency of the Full Width at Half Maximum (FWHM) of (111) peak of the growth films to increase probably due to all of the possible RE^{3+} species present in Cd^{2+} sites and interstitials positions [22], and also to the existence of RE_2S_3 , which distort the crystalline lattice and provoke disorder. The distortion produces a strong strain that affects the interatomic distances; this similar fact has been reported [16,23]. In this work, the strain and distortion of the lattice can be smaller. The appearing of S^{2-} ions into the material favours the relaxing of the lattice. Transmission electron microscopy (TEM) measurements on the synthesised samples were carried out, which corroborate the presence and the nanometric size of particles. In Fig. 4 are shown TEM micrographs of three typical samples (M65, M100 and M115). From them is evident the presence of particles with almost completely spherical shape of nanometric size. Based on hundreds of measurements taken from the TEM micrographs of the typical samples size distribution histograms were obtained, which are shown in the insets, and in them can be detected a Gaussian adjustment with a narrow distribution of size and maximum values of 5.44, 3.55 and 3.22 nm. Absence of a bimodal size distribution in the size distribution histograms suggests that the nanoparticles obtained by the synthesis process at different times correspond to the formation of an CdS:RE³⁺ system and not the physical mixture of nanoparticle sizes. A comparable analysis was performed for some of the samples and the results are listed on Table II. Larger semiconductor nanoparticles are obtained of the undoped CdS and smaller with doped CdS. Therefore, the synthesis time can be used to control the formation and size of the doped CdS nanoparticles. As can be observed in Table II, the particle size values obtained from the Debye-Scherrer equation and those measured from the TEM micrographs have small discrepancies. These slight discrepancies in particle sizes are due to some approximations involved in the calculations using the Debye-Scherrer equation or coalescence of nanocrystals during preparation for analysis by TEM. With the purpose of verifying the

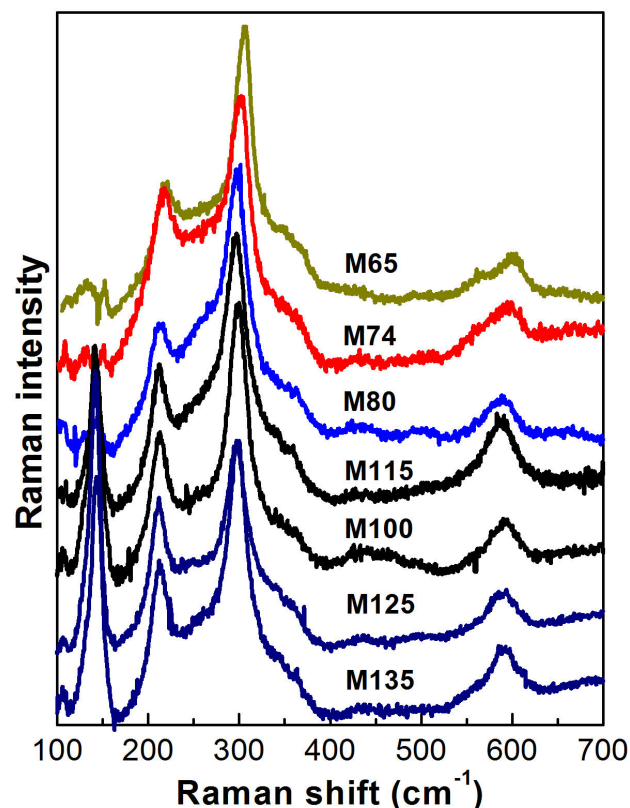


FIGURE 5. a) Room temperature Raman spectra of some synthesized CdS nanofilms.

structure's quality and crystalline phase of the synthesised semiconductor nanoparticles, HRTEM images were taken and the results are included in the inset of Fig. 4, which are the result of the processing of the HRTEM image using filters in Fourier space. From the HRTEM micrographs of the typical samples, it is clearly observed the formation of nanoparticles with a defined crystalline structure, zinc blende type. Amplifying and analysing the selected area of the micrograph, which is shown as insets in Fig. 4, it was possible to calculate the interplanar distances of 0.33 nm corresponding to plane (111) of particles of crystallized CdS in zinc blende type crystalline phase. As can see, the results obtained by HRTEM are in good agreement with the results calculated from X-ray diffraction studies.

Figure 5 illustrates the Raman spectra of typical nanofilms, which have nearly the same features in the investigated range. Each of the phonon wavenumber was extracted by fitting the Raman spectrum to a Lorentz line shape, the 1LO and 2LO phonons and multiphonon processes can be clearly observed, which correspond a zinc blende (ZB) type crystalline phase as was obtained by X-ray diffraction. Raman scattering shows that the lattice dynamics is characteristic of bimodal behaviour and the multippeak adjust of the first optical longitudinal mode denotes the CdS. The Raman spectra exhibit relatively sharp crystal-like peaks. In Fig. 6 Raman spectra of three typical samples are displayed. The Raman shift of single CdS (nanoparticles), M65 sample, ap-

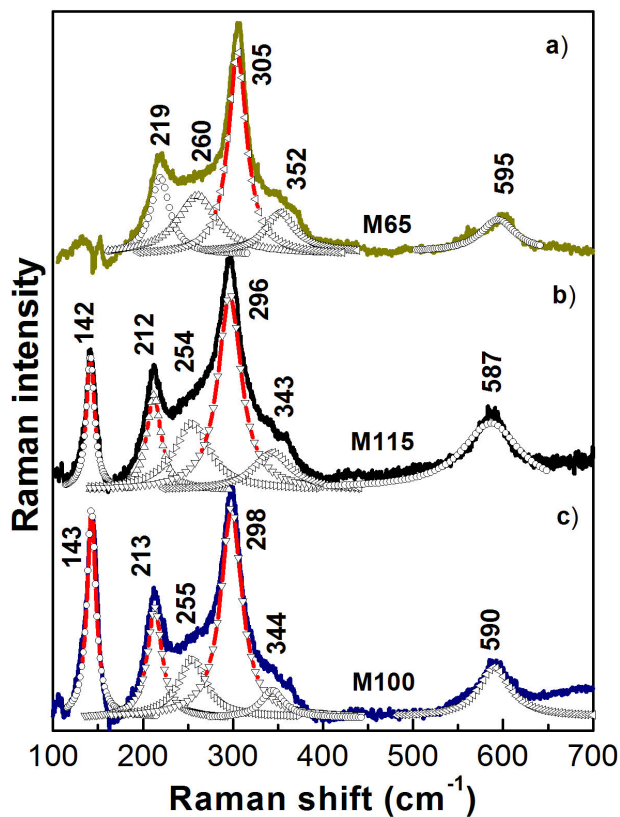


FIGURE 6. Deconvolution of the Raman spectra for three samples: a) M65, b) M115 and c) M100. The -o- lines are their respective fitting.

appears at $\sim 305 \text{ cm}^{-1}$ that is attributed to the $A_1(\text{LO})$ mode (where LO is a longitudinal optical phonon) with a full width at half maximum (FWHM) of ca. 24.82 cm^{-1} . The 1LO Raman shift of $\text{CdS}:\text{Ce}^{3+}$ (nanoparticles), M100 sample, appears at $\sim 298 \text{ cm}^{-1}$ with a FWHM of ca. 27.91 cm^{-1} . Finally, the 1LO Raman shift of $\text{CdS}:\text{Eu}^{3+}$ (nanoparticles), M115 sample, appears at $\sim 296 \text{ cm}^{-1}$ with FWHM of ca. 30.84 cm^{-1} . As is observed of these results $A_1(\text{LO})$ mode redshifts slightly as the RE's are incorporated. Additionally, the slight increase of the FWHM to higher synthesis times can be attributed to a slight deterioration of the crystallinity of the CdS nanocrystals due to the incorporation of RE to Cd sub-lattice. As has been reported that a defect-free crystalline CdS film should have a FWHM of 8.0 cm^{-1} [24]. Therefore, synthesized nanofilms contain a high density of crystalline defects. In addition, to the 1LO phonon and its phononic replicas for M65 sample, several vibrational bands are resolved at 219, 260 and 352 cm^{-1} suggesting that the samples have better crystalline quality [25]. The vibrational bands can be assigned to multiphonon scattering, which is consistent with reported works [26,27]. The feature at the high-energy shoulder, which is very weak peak at 352 cm^{-1} , which is the subject of a recent study by Dzhegagan *et al.* [28], who suggest that it results from the participation of acoustic phonons to the scattering process and the mode corresponding to the low-energy shoulder originates from surface optical

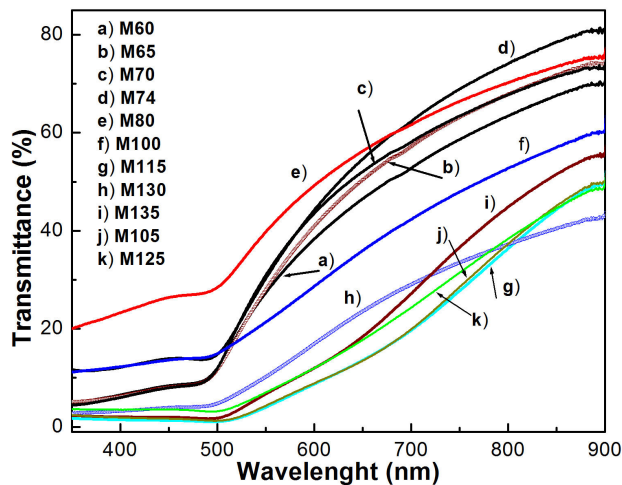


FIGURE 7. It illustrates the transmittance spectra of some typical samples, which were measured at room temperature.

phonon modes (SO) at 260 cm^{-1} [29,30] and it can be assigned to E_2^H [31]. The peak at approximately 219 cm^{-1} can be assigned to multiphonon scattering, which is consistent with other reports [27]. As is observed in Fig. 6, the frequencies of the vibrational bands decrease as the RE molar fraction increases, this is consistent because the ionic radius of RE is higher. In addition, it observes that the Raman spectra of doped CdS present a vibration mode around 142 cm^{-1} well-resolved that can be associated to the combination of longitudinal and transverse acoustic phonon modes in RES nanocrystals [32], which depend strongly on the RE molar fraction. Besides, it is observed that these bands happened a redshift. Similar vibration modes were obtained by Raman theories and are in agreement with the results of de Wijs *et al.* [33]. The effect of doping by rare earths on the optical properties of doped CdS nanofilms was investigated by room temperature transmittance as function of the synthesis time. The transmittance spectra in the visible and infrared ranges are recorded for the nanofilms in the wavelength range 350–1100 nm, which are illustrated in Fig. 7. The sharp reduction in the transmittance spectra at the wavelengths lower than 500 nm is due to the fundamental absorption edges of the different films. The $\text{CdS}:\text{RE}^{3+}$ nanofilms were transparent, with no observable blue colouration under our experimental conditions. The main band shifts slightly to red as $V[\text{RE}^{3+}]$ increases. The slight reduction of the main absorption edge is indicative of the compensation of broken bonds, but also it indicates that the RE atoms are being incorporated into interstitials of the unit cell, see Table II. In order to M135 sample the optical band gap decreased slightly by about 84.22 meV compared with the band gap energy of the M60 sample, which can be related to RE^{3+} incorporation to the molecule and the average grain size. This band gap decrease can be explained due to the substitution in the lattice of cadmium atoms (ionic radii $\sim 0.95 \text{ \AA}$) by cerium (ionic radii 1.15 \AA) and europium (ionic radii 1.09 \AA) atoms that are higher. The intrinsic absorption edge of the $\text{CdS}:\text{RE}$ nanofilms could be evaluated and discusses in terms of the indirect interband transition. As

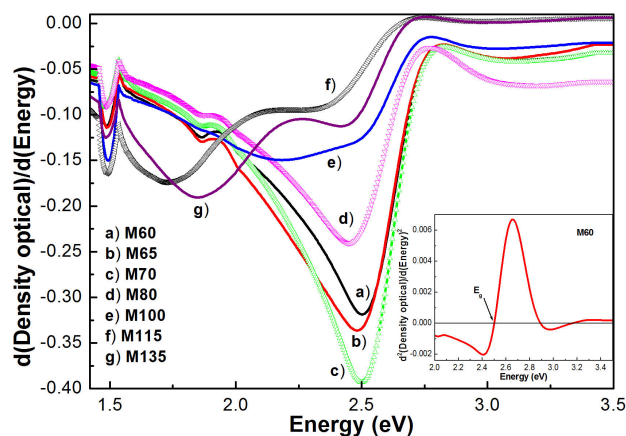


FIGURE 8. It is shown the first derivative of the optical absorption (OD) as a function of the photon energy ($h\nu$), for some typical samples with different synthesis time values. The inset displays the second derivative of OD versus E , which allows calculate the band gap energy. The downward arrow points out the position of the E_g value for M60 sample.

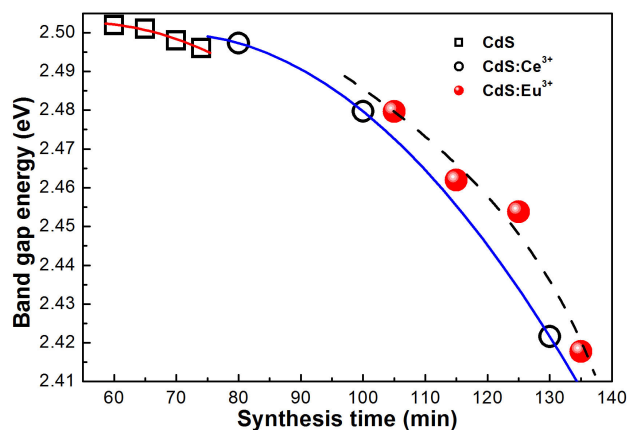


FIGURE 9. It shows band gap energy as a function of synthesis time for three samples series that were estimated by transmittance.

is well-known the optical band gap (E_g) of a semiconductor material is related to the optical absorption coefficient (α) and the incident photon energy (E). The band gap energy (E_g) for the different synthesis times was calculated from optical transmittance data. Figure 8 shows the first derivative of the optical density [$d(OD)/dE$] as a function of the incident photon energy (E) of typical samples. The relative minima in the transmittance spectra of the first derivative $d(OD)/dE$ versus E graph define the critical points of the band structure [34,35], which are associated absorption bands due impurities and vacancies [16]. The inset of Fig. 8 illustrates the second derivative of OD plotted against E of typical samples. A more precise position of the critical point E_g in the E -axis is defined by the crossing of the second derivative curve with the E axis. The estimated optical band gap of the undoped CdS nanofilms, M65 sample, is of 2.50 eV that corresponds to pure CdS and is 91 meV higher than band gap in CdS bulk,

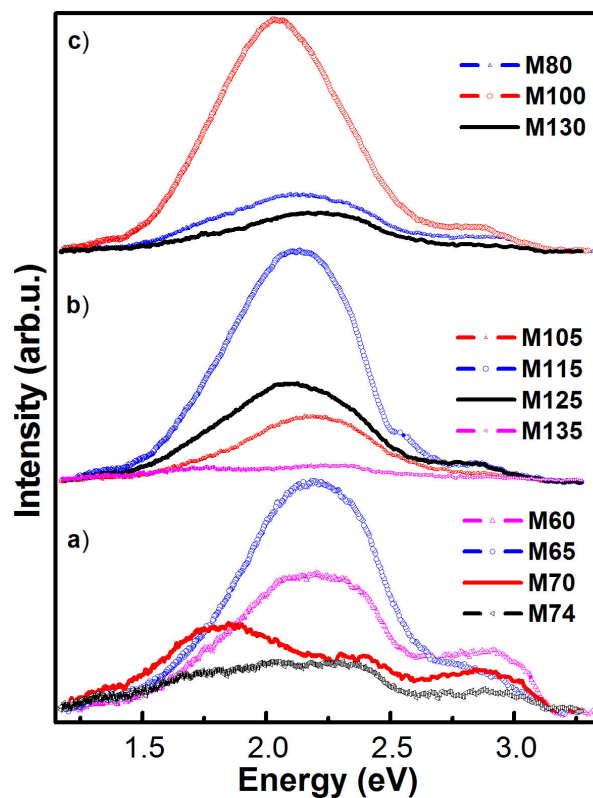


FIGURE 10. It shows the photoluminescence spectra CdS for three nanofilms series: a) undoped CdS, b) Eu-doped CdS and c) Ce-doped CdS.

which is indicative that there is quantum confinement. This discrepancy is associated to the average grain size [36,37]. As is observed in the inset of Fig. 8 band gap energy redshifts lightly with the $V[RE^{3+}]$ increase or that is the same with the increase of the synthesis time. These values are shown in Fig. 9.

Figure 10 shows the photoluminescence spectra of the undoped CdS for four different synthesis times. Figure 11 shows the photoluminescence spectra the deconvolution of three typical samples (M65, M100 and M115). For sample M65, which presents best luminescence of undoped films, the radiative bands are observed at 2.86, 2.37, 2.19, 1.88 and 1.38 eV that are labelled by a, b, c, d and e in the PL spectrum for a better discussion, see Fig. 11A. The band a is associated a radiative transition band-to-band, which is higher than the undoped CdS band gap for 366 meV. This is due to the quantum confinement associated with grain size since it is less than the excitonic Bohr radius. The band b is clearly identified on as-grown CBD-CdS at 2.37 eV, which is called the optical signature of interstitial oxygen [38]. Its relative intensity increases with the synthesis time until it reaches a maximum at 65 min and then decreases for longer times, as is observed in figure. It has reported that in samples grown by close-spaced sublimation (CSS) technique the effect of oxygen leads to the appearance of a band at 2.2 eV [38]. The band c could be attributed to the CdO complexes that would be

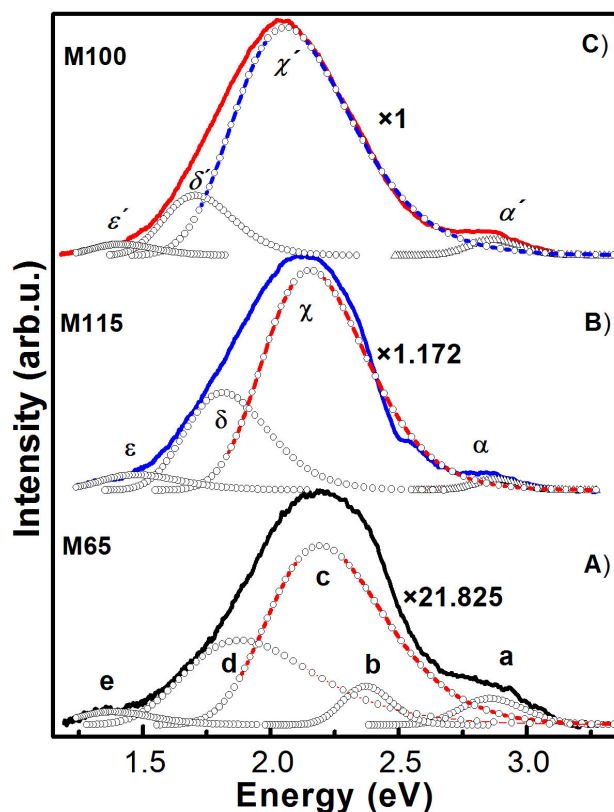


FIGURE 11. It is illustrated the PL deconvolution of the CdS nanofilms that presented the most intense photoluminescence: A) M65 sample, B) M115 sample and C) M100 sample. Additionally, it is shown the passivation factor associates to incorporation rare earth.

formed during the growth due to the presence of oxygen during the nucleation of the layer, since the CdO band gap is about 2.16 eV [39]. For four studied CBD-CdS samples, another broad band, band d, is observed around 1.88 eV, this band named the “orange band” has been observed between 2.03-2.08 eV [40,41], it is possibly associated to a donor-acceptor pair (DAP) radiative transition between a donor level related to interstitial cadmium (I_{Cd}^{2+}) and an unidentified acceptor level. The ionization energy of this donor has estimated to be between 0.12 and 0.26 eV, which corresponds to (I_{Cd}^{2+}) [38]. Finally, the broad and weak peak (band e) observed at 1.39 eV, which disappears when synthesis time increases, it is in the infrared region and is associated with unidentified deep impurities. In addition, Fig. 10a shows the behaviour of the PL spectra intensities of the four undoped CdS nanofilms, where it is clearly observed that the dominant spectrum is obtained at 65 min of synthesis time, sample M65, and for other times are weaker. Fig. 10b the photoluminescence spectra of the Eu^{3+} -CdS samples are shown. It is clearly observed that in the PL spectra the band called the optical signature of interstitial oxygen at 2.37 eV is not present, which is indicative that the incorporation of rare earths decreases the concentration of interstitial oxygen. The photoluminescence spectrum of the M115 nanofilm, which exhibits radiative transitions at 2.88, 2.15,

1.81 and 1.48 eV, labelled by α , χ , δ and ε , see Fig. 11B. The emission peak α was clearly observed, which is associated to radiative transition band-to-band. This band has been related to the radiative transition of CdS nanostructures into band-edge and surface defects due to the quantum confinement effect because of grain size is lower than the exciton Bohr radius, which is higher by 409 meV than the band gap. The dominant radiative peak χ has been associated to the intra-4f radiative transitions of Eu^{3+} ions that corresponds to the magnetic dipole transition (${}^5\text{D}_0 \rightarrow {}^7\text{F}_1$), which was blue shifted compared to previous results [38,42]. In Eu^{3+} -doped CdS, the ${}^5\text{D}_0 \rightarrow {}^7\text{F}_1$ transition is mainly magnetically allowed (magnetic-dipole transition). The surface-defect radiative transitions are caused by surface states, such as sulphur vacancies and/or sulphur dangling bonds created by doping are in the energy range 1.77-2.48 eV [38], for which the peak δ is associated with surface defects of the CdS nanocrystals. Finally, the peak ε is in the region of low energies, which is associated at residual impurities. The peak χ is the one that increases more its intensity with the synthesis time, reaching a maximum at 115 min and then decreasing. These observations indicate that a part of Eu^{3+} ions, contained in CdS nanocrystals and the energy can be significantly transferred from the host CdS to Eu^{3+} ions [43,44]. Upon excitation, the energy from non-radiative recombination of electron-hole pairs can be transferred to the high energy levels of the Eu^{3+} ions [45,46]. The mechanism of the intensification of rare earth emission (REE) has already been reported [46], which also supports the observed results of the present study. These results indicate that the adsorbed CdS particles significantly influence the excitation of 4f electrons in rare-earth ion. A significant change in the intensity of the emission bands was observed for the samples prepared using different synthesis time, which are due to the variation in the structures. It may also be attributed to the change in the energy transfer rate with particle size variation and the shape of the nanocrystals. Figure 10c shows the photoluminescence spectra of the Ce-doped CdS, which are very similar to those obtained with the Eu^{3+} -doped CdS. Sample M100 photoluminescence spectrum presents radiative bands at 2.87, 2.06, 1.71 and 1.42 eV, called α' , χ' , δ' and ε' , see Fig. 11C. The radiative band α' corresponds to the band-band transition. The band χ' is the most intense of PL spectrum, which is associated to Ce incorporated to the sub-lattice of Cd. Therefore, it is considered that the radiative transitions present in the luminescence of the Ce^{3+} -doped CdS have the same origin as those present in the PL of the Eu^{3+} -doped CdS and their redshift is due to the ionic radius of the Ce^{3+} is higher than the Cd, which strains the lattice.

In addition, Fig. 11 shows the comparison of the photoluminescence spectra of the three samples with the best luminescence results, undoped and doped with rare earths CdS. It is clearly observed that the intensity of the PL spectra of doped CdS increases considerably, indicating that there is a passivation of the surface state density of the nanocrystals, but their dominant band redshifts.

4. Conclusions

In this work reported the growth successfully of (Eu³⁺, Ce³⁺)-doped CdS nanostructures synthesised by chemical bath deposition technique at different synthesis times and at 70 ± 2°C. The crystalline structure of the nanostructures was zincblende type (111) direction, which was obtained by X-ray diffraction and Raman spectroscopy. The incorporation of rare earths in the CdS lattice was confirmed by EDS and X-ray diffraction. The nanocrystal size was determined by the Debye-Scherrer equation from ZB (111) direction, which was ranged from 2.35 to 2.67 nm for the CdS and 1.84-2.33 nm for rare earth-doped CdS that was confirmed by TEM. These grain sizes confirmed the quantisation effect in the synthesized samples due to are lower than the exciton Bohr radius. The RE-doped CdS exhibits a direct band gap that slightly decreases with increase of the synthesis time, from 2.50 to 2.42 eV, which was obtained by transmittance measurements. The room temperature photoluminescence of the undoped CdS presents the band-band transition associated to CdS nanocrystals size and the radiative transitions associated with residual impurities and structural defects, mainly the optical signature of interstitial oxygen. The photoluminescence of samples doped with

europium present the band-band transition, in addition the radiative band associated to the intra-4f radiative transitions of Eu³⁺ ions that corresponds to the magnetic dipole transition (⁵D₀ → ⁷F¹). For the case of cerium-doped samples, the results obtained were similar to those for europium. The results confirm that at least a part of the Eu³⁺ ions is effectively doped into CdS nanocrystals and the energy transfer occurs from CdS nanocrystals to Eu³⁺ ions. It was observed that the nanostructure, crystallite size and the band gap of the europium and cerium doped CdS nanocrystals can be finely controlled by simply varying the synthesis time. The passivation of the CdS by rare earths was approximately of an order of magnitude obtaining better results with cerium.

Acknowledgments

The authors thank SIP-IPN for their support for the development of this work. Another author wishes to thank the CONACYT programs that strengthen the scientific and human effort of the authors for the scholarship received. The authors wish to thank Miss Janet Flores-Martínez for her technical support and valuable discussions that made this research possible.

1. J.W. Stouwdam, G.A. Hebbink, J. Huskens, F.C.J.M. van Veggel, *Chem. Mater.* **15** (2003) 4604.
2. G. Blasse, B.C. Grabmaier, *Luminescent Materials*. (Ed. Springer Verlag Berlin Heidelberg 1994).
3. M.J.F. Digonnet, *Rare-Earth-Doped Fiber Lasers and Amplifiers. Revised and Expanded*. (Marcel Dekker, Inc. New York. 2001).
4. R. Reisfeld, C.K. Jørgensen, *Lasers and excited states of rare earths*. (Springer-Verlag, New York. 1977).
5. M. Konishi, T. Isobe, M. Senna, *J. Lumin.* **93** (2001) 1.
6. A. Chowdhuri *et al.*, *Appl. Phys. Lett.* **84** (2004) 1180.
7. P. Yang, K.N. Liou, M.I. Mishchenko, B.C. Gao, *Appl. Opt.* **39** (2000) 3727.
8. D.T. Simon, M.R. Geller, *Phys. Rev. B* **64** (2001) 115412.
9. M.K. Jayaraj and C.P.G. Vallabhan, *J. Electrochem. Soc.* **138** (1991) 1512.
10. J. Liqiang *et al.*, *J. Solid State Chem.* **177** (2004) 3375.
11. A. Vij *et al.*, *J. Phys. D: Appl. Phys.* **42** (2009) 105103.
12. V. Kumar *et al.*, *J. Appl. Phys.* **107** (2010) 123533.
13. Q.Q. Liu *et al.*, *Physica B* **405** (2010) 4360.
14. S. Radhu and C. Vijayan, *Mater. Chem. Phys.* **129** (2011) 1132.
15. W.Q. Peng, G.W. Cong, S.C. Qu, and Z.G. Wang, *Nanotechnology* **16** (2005) 1469.
16. J. Díaz-Reyes *et al.*, *Braz. J. Phys.* **46** (2016) 612.
17. M. Guglielmi, A. Martucci, J. Fick, and G. Vitrant, *J. Sol-Gel Sci. Technol.* **11** (1998) 229.
18. J.A. Lange's, *Handbook of Chemistry* (McGraw Hill Book Co., Beijing, 1999).
19. J.A. Dean and Lange's, *Handbook of Chemistry*, 13th ed. (New York: McGraw-Hill. 1987).
20. R. Ortega-Borges and D. Lincot, *J. Electrochem. Soc.* **140** (1993) 3464.
21. M. Grus and A. Sikorska, *Physica B* **266** (1999) 139.
22. J. Díaz-Reyes *et al.*, *Mat. Sci. Semicond. Proc.* **37** (2015) 199.
23. M. Esmaili, A. Habibi-Yangjeh, *Chin. J. Catal.* **32** (2011) 933.
24. M. Froment, M.C. Bernard, R. Cortes, B. Makili, and D. Lincot, *J. Electrochem. Soc.* **142** (1995) 2642.
25. V. Sivasubramanian, A.K. Arora, M. Premila, C.S. Sundar, and V.S. Sastry, *Physica E: Low-dimensional Systems and Nanostructures* **31** (2006) 93.
26. C. Hu, X. Zeng, J. Cui, H. Chen, and J. Lu, *J. Phys. Chem. C* **117** (2013) 20998.
27. S. Kar, B. Satpati, P.V. Satyam, and S. Chaudhuri, *J. Phys. Chem. B* **109** (2005) 19134.
28. V.M. Dzhegagan, I. Lokteva, M. Ya. Valakh, O.E. Raevska, J. Kolny-Olesiak, and D.R.T. Zahn, *J. Appl. Phys.* **106** (2009) 084318.
29. F. Comas, N. Studart, and G.E. Marques, *Solid State Commun.* **130** (2004) 477.
30. H. Lange, M. Artemyev, U. Woggon, and C. Thomsen, *Nanotechnology* **20** (2009) 045101.
31. H.M. Fan *et al.*, *Appl. Phys. Lett.* **91** (2007) 171911.

32. G.D. Smith, S. Firth, R.J.H. Clark, and M. Cardona, *J. Appl. Phys.* **92** (2002) 4375.
33. G.A. de Wijs, and R.A. de Groot, *Electrochim. Acta* **46** (2001) 1989.
34. B.G. Potter Jr., and J.H. Simmons, *J. Appl. Phys.* **68** (1990) 1218.
35. L. Katsikas, A. Eychmüller, M. Giersig, and H. Weller, *Chem. Phys. Lett.* **172** (1999) 201.
36. D.J. Seo, *J. Korean, Phys. Soc.* **45** (2004) 1575.
37. B.J. Jin, H.S. Woo, S. Im, S.H. Bae, and S.Y. Lee, *Appl. Surf. Sci.* **169/170** (2001) 521.
38. F. Gemain, I.C. Robin, S. Renet, and S. Bernardi, *Phys. Status Solidi C* **9** (2012) 1740.
39. P.H. Jefferson *et al.*, *Appl. Phys. Lett.* **92** (2008) 022101.
40. K. Mochizuki, M. Satoh, and K. Igaki, *Jpn. J. Appl. Phys.* **22** (1983) 1414.
41. A. E. Abken, D. P. Halliday, and K. Durose, *J. Appl. Phys.* **105** (2009) 064515.
42. A. Patra *et al.*, *J. Phys. Chem. B* **103** (1999) 3361.
43. T. Hayakawa, S.T. Slevan, and M. Nogami, *Appl. Phys. Lett.* **74** (1999) 1513.
44. K. Singh, S. Kumar, N.K. Verma, and H.S. Bhatti, *J. Nanopart. Res.* **11** (2009) 1017.
45. J. Del Castillo, V.D. Rodríguez, A.C. Yanes, J. Méndez-Ramos, and M.E. Torres, *Nanotechnology* **16** (2005) S300.
46. R. Reisfeld, M. Gaft, T. Saridarov, G. Panczer, and M. Zelner, *Mater. Lett.* **45** (2000) 154.